THE JOURNAL OF PHYSICAL CHEMISTRY B

ARTICLE

pubs.acs.org/JPCB

Insight into Asphaltene Nanoaggregate Structure Inferred by Small Angle Neutron and X-ray Scattering

Joëlle Eyssautier,[†,‡] Pierre Levitz,[‡] Didier Espinat,[†] Jacques Jestin,[§] Jérémie Gummel,[∥] Isabelle Grillo,[⊥] and Loïc Barré*[,†]

[†]IFP Energies nouvelles, 1-4 av. de Bois-Préau, 92852 Rueil-Malmaison Cedex, France

[‡]Physique de la Matière Condensée, CNRS—École Polytechnique, UMR 7643 CNRS, 91128 Palaiseau Cedex, France

[§]Laboratoire Léon Brillouin, LLB, CEA Saclay, 91191 Gif-sur-Yvette Cedex, France

[∥]European Synchrotron Radiation Facility, ESRF, BP 220, 38043 Grenoble Cedex 9, France

[⊥]Institut Laue Langevin, ILL, 6 rue Jules Horowitz, BP 156 38042 Grenoble Cedex 9, France

Supporting Information

ABSTRACT: Complementary neutron and X-ray small angle scattering results give prominent information on the asphaltene nanostructure. Precise SANS and SAXS measurements on a large *q*-scale were performed on the same dilute asphaltene−toluene solution, and absolute intensity scaling was carried out. Direct comparison of neutron and X-ray spectra enables description of a fractal organization made from the aggregation of small entities of 16 kDa, exhibiting an internal fine structure. Neutron contrast variation experiments enhance the description of this nanoaggregate in terms of core−shell disk organization, giving insight into core and shell dimensions and chemical compositions. The nanoaggregates are best described by a disk of total radius 32 Å with 30% polydispersity and a height of 6.7 Å. Composition and density calculations show that the core is a dense and aromatic structure, contrary to the shell, which is highly aliphatic. These results show a good agreement with the general view of the Yen model (Yen, T. F.; et al. *Anal. Chem.* **1961**, *33*, 1587−1594) and as for the modified Yen model (Mullins, O. C. *Energy Fuels* **2010**, *24*, 2179−2207), provide characteristic dimensions of the asphaltene nanoaggregate in good solvent.

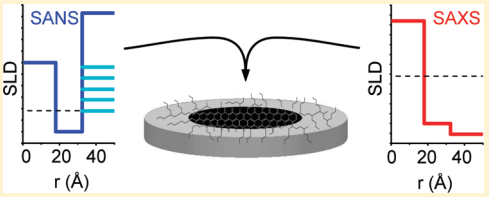

I. INTRODUCTION

Asphaltenes are the enigmatic fraction of petroleum, and their structure−function relationships have long been of interest. Known to increase the oil viscosity, they are also blamed for plugging the pores of reservoirs and catalytic networks.[1,2] Their diffusivity is reduced because of aggregation mechanisms which still remain to be understood. Their definition is based on a solubility class: they represent the *n*-heptane insoluble part of crude oil. This definition gives rise to highly aromatic molecules (H/C ∼ 1) of complex and polydisperse structure. A consensus is forming on their molecular weight. Most studies tend to agree on a value peaking at 750 Da, with a full width at half-maximum of 500−1000 Da.[3] The asphaltene molecule is described with a "like a hand" or "continental" view, made of an aromatic core of several rings, surrounded by more or less extended alkyl chains. This island model is supported by various techniques such as fluorescence spectroscopy.[4] This representation is opposed in literature to the so-called "archipelago model", historically deduced from chemical and thermal bulk degradation studies,[5] although subjected to major artifacts. This type of molecule represents several fused-ring systems that are interconnected by alkyl chains. These two molecular structures probably coexist, and the debate is now centered on their proportions and specific roles within an asphaltene mixture.

Asphaltenes have been studied with a colloidal approach by numerous techniques, describing the system at various length scales. In the early 1960s, Yen was a pioneer in presenting a hierarchical picture of asphaltenes, showing aggregation mechanisms from the molecular state to the cluster state.[6,7] This promising model was mainly figured out on solid asphaltene characterization data, from XRD measurements highlighting aromatic stacking, with aggregation numbers between 5 and 8.[7−9] However, typical sizes and experimental background often lack to this Yen model, in particular for asphaltene solutions. Results supported by molecular simulations give rise to similar aromatic stacking of various aromatic model compounds,[10−12] mostly represented by the island molecular model.

Nanoaggregates, formed from the self-association of molecular aromatic sheets, are commonly considered. Property changes were observed with an increasing concentration, which is usually associated with the limit of a primary aggregation of the molecules at very low concentration. This limit is defined as the nanoaggregate concentration (NAC), occurring between 50 and 200 mg/L.[13−19]

Received: December 2, 2010
Revised: April 4, 2011
Published: May 10, 2011

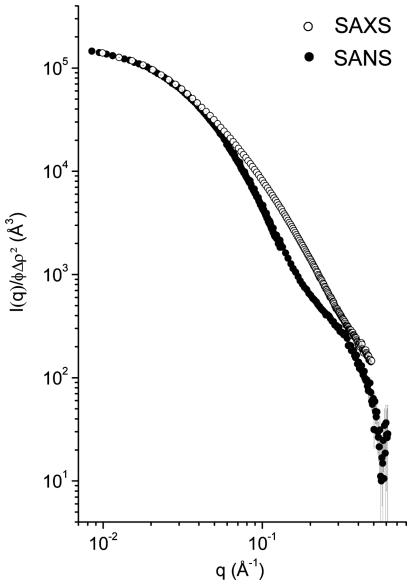

Figure 1. SANS (●) and SAXS (○) spectra of a 5 g/L asphaltene solution in D- and H-toluene respectively. Intensities are normalized by the mean contrast term and the asphaltene volume fraction.

Most of the techniques trying to identify the nanoaggregates use hydrodynamic properties, measuring the diffusion coefficient of the particles, notably NMR among others. Values between 1 and 4 × 10^{-10} m^2/s were found,[13,15−17,20−24] giving rise to equivalent hydrodynamic sphere radii between 10 and 36 Å. All these results converge to an aggregation number equal to 8.[19,25] However, no structural organization was experimentally described in liquid condition where nanoaggregate diffusion is observed.

These numerous additional results characterizing the sizes of asphaltene molecules and nanoaggregates in solution gave rise to the "modified Yen model",[26] which brings subsequent details on the hierarchical asphaltene organization, very close to the view of Yen. A more precise idea is given on molecular weights, sizes and aggregation numbers at different stages, thanks to a large literature review on various measurements in solutions.

The small angle neutron and X-ray scattering (SANS, SAXS) technique was intensively applied on dilute asphaltene solutions. From experimental data, two approaches are usually presented to extract geometrical parameters such as shape, characteristic dimensions and polydispersity. Using the Guinier or the Zimm approximation, radii of gyration (R_g) and molecular weight (M_w) can be extracted from the low-angle region analysis. Reported R_g values are between 40 and 60 Å, and M_w are around 50,000 Da.[27−32]

The other approach consists of modeling the experimental spectra in the whole q range assuming the shape of the particles. This method is widely applied, and various form factors were fitted to asphaltenes' SAXS and SANS spectra: polydisperse thin disks,[33] spheres,[34] ellipsoids and spheres,[35] polydisperse spherical and oblate cylinders, swollen mass fractal model.[30,36] But this model-dependent method has major drawbacks, introduced first from the choice of the presumed form factor and polydispersity function and second from the high number of adjustable parameters.[37] Barré et al.[38] have also demonstrated that different models (spheres, disks or ellipsoids) are able to fit the experimental SAXS data. In this context, the use of complementarities between SAXS, SANS, and other techniques like viscosity[27,29] appears to be a powerful way to resolve the problems of unity of solutions described below.

In the dilute regime, SAXS and SANS measurements of radii of gyration described earlier are unequivocal, as well as molecular weights. One has to notice that the reported values for asphaltenes (∼60 Å) are larger than the nanoaggregates described from hydrodynamics (∼20 Å). As described by Barré et al.,[27] these radii of gyration provide a good estimation of the size of a mass-fractal structure induced by the aggregation of smaller entities. However, the characterization of these nanoaggregates, of typical size 20 Å, with small angle scattering requires exploration of the sample on a wider length scale toward the high q values. As noticed,[30] low intensities measured at high q values are difficult to extract from background signal.

As an introduction to the work presented here and to give insight into a nanoaggregate structure, SANS and SAXS spectra of an asphaltene solution are shown in Figure 1, over a wide q range toward the high q values. As previously observed by Barré et al.,[39] the two spectra superimpose at small q values, meaning that asphaltenes are homogeneous objects at large length scale. However, in the high q range, the spectra differ significantly: asphaltene particles present heterogeneities at small length scale. While the X-ray spectrum exhibits a smooth power law, the neutron spectrum presents an oscillation, which is characteristic of a fine structure.

This literature review reveals the complexity of the asphaltene system, with a lot of parameters to be determined. The aim of this work is to acquire experimental small angle scattering data for several solvent conditions in order to increase the number of data. Restrictive conditions will be applied to the model curve fitting in order to increase the chances of reaching the unique solution. A quantitative and comparative analysis of neutron and X-ray spectra is proposed taking into account the hierarchical structure of the asphaltene aggregate, the polydispersity and the heterogeneous organization of the asphaltene molecules on the nanoscale. Our results in terms of dimensions and composition will be compared with the literature data. The limits, the selectivity and the possible improvement of our model will be finally addressed.

II. EXPERIMENTAL SECTION

1. Asphaltene Sample Preparation and Characterization. Asphaltenes were prepared by precipitation in an excess of *n*-heptane (NF-T60-115 method) from an asphaltene-rich Safaniya vacuum residue (VR) coming from a Saudi Arabian field. The precipitate was then washed with a Soxhlet-type apparatus (Kumagawa) at *n*-heptane boiling temperature (98 °C), until the solvent was clear (∼4 h). The asphaltene C7 thus obtained corresponds to 15%w of the VR. Density measurements were done with an Anton Paar DMA5000 densitometer at 20 °C. The specific volume of solutions versus the asphaltene mass fraction shows a linear trend in the range 0.01−25% which allows extrapolation to null dilution. Table 1 shows asphaltenes' physical and chemical properties.

Samples were prepared by mixing asphaltene powder in the specific amount of H-toluene (Rectapur grade, VWR International) for SAXS measurements (5 g/L), D-toluene (Eurisotop) for SANS (5 g/L) and toluene at various H/D ratio for neutron contrast variation experiments (50 g/L). Anhydrous toluene was prepared with a 4 Å molecular sieve when working at low asphaltene concentration (5 g/L). Indeed, water molecules can

Table 1. Asphaltene Chemical and Physical Properties

chemical composition (% wt)	C	82.6
	H	7.6
	N	1.0
	O	1.3
	S	7.6
aromaticity	H/C	1.09
mass density (g/cm^3)		1.195

be bound to the asphaltene molecules,[40] which can affect their aggregation mechanism. When working at low asphaltene concentration, it is required to eliminate water traces. All samples were prepared a week before experiments to avoid kinetic effects.

2. Small Angle X-ray Scattering. Small angle X-ray scattering measurements were done on the ID02 instrument at the European Synchrotron Radiation Facility in Grenoble, France. The detector is a Frelon 4 M CCD camera with a 2048 × 2048 pixel chip of a total 10 × 10 cm^2 surface. Due to the weak scattering of dilute solutions of asphaltene, a 4 × 4 binning has been used to increase the statistic. The sample-to-detector distance used was 1 m along with a 0.1 nm wavelength X-ray beam, giving a q range lying from 1×10^{-2} Å^{-1} to 5×10^{-1} Å^{-1}. All measurements were done under atmospheric pressure and at room temperature in a single quartz capillary to ensure good subtraction of the background.

During the acquisition, standard corrections are made for X-ray beam transmission and monitor, detector efficiency and distortion and applied to the recorded CCD image. A measurement of pure water is done to calibrate the instrument, and it allows getting the scattered intensities in absolute units after division by the thickness of the sample. SAXS 2-D images are then azimuthally regrouped after applying a mask to remove faulty regions of the image (essentially due to the beam-stop). To get the signal of asphaltene, a measurement of the capillary filled with the corresponding solvent is done to subtract the background signal due to the parasitical scattering of the direct beam, the capillary and the solvent. This final subtraction gives a $I = f(q)$ curve of asphaltene in solution in absolute intensity.

3. Small Angle Neutron Scattering. SANS measurements were carried out at the Laue Langevin Institute (ILL, Grenoble, France) on the D22 spectrometer, and the contrast variation experiments were performed at the Laboratoire Leon Brillouin (LLB, Saclay, France) on the PAXE instrument.

The D22 detector is composed of an array of 128 vertical independent counter tubes, covering a surface of 1 m^2. We worked at a fixed wavelength of 6 Å and two sample-to-detector distances (4 m and 8 m) covering a total q range of 6×10^{-3} to 6×10^{-1} Å^{-1}. Data processing was performed following the standard D22 procedures[41] with H_2O as absolute intensity calibration standard. The scattering intensities were normalized to the monitor, the cell thickness and the transmission. The incoherent scattering background was measured at high q, and the plateau was subtracted from the sample. Samples and solvents were measured in 5 mm Hellma quartz cells. Solvent subtraction was done by subtracting the plateau obtained at very high q values.

The PAXE detector is an XY multidetector filled with BF_3. We worked at a fixed wavelength of 4 Å, and the sample-to-detector distance was 1.14 m, covering a total q range of 6×10^{-2} to 6×10^{-1} Å^{-1}. Data processing was performed following the standard PAXE procedures. Absolute intensity was obtained by measuring the incident flux. The scattering intensities were normalized by the monitor, the cell thickness and the transmission. Samples and solvents were measured in 2 mm Hellma quartz cells, and pure solvent signal was subtracted weighted by the asphaltene concentration. Incoherent scattering, introduced by the high asphaltene concentration (50 g/L), was subtracted according to the procedure detailed in Supporting Information, part A.

III. SMALL ANGLE SCATTERING

The experimental quantity observed in a small angle scattering experiment is the intensity in terms of the coherent macroscopic cross section $(d\Sigma/d\Omega)$ as a function of the scattering vector $q = [4\pi/\lambda] \sin(\theta/2)$, with λ being the radiation wavelength and θ being the scattering angle. q has the dimension of a reciprocal length and can therefore be regarded as an inverse meter stick. The equation describing the scattering cross section of polydisperse and anisotropic particles can be written according to the "decoupling approximation"[42,43] as

$$\frac{d\Sigma}{d\Omega}(q) = I(q) = N_P \langle P^2(q) \rangle S'(q) \quad (1)$$

Here, N_P is the average number density of scattering particles; V_P is the average volume of one particle. N_P can be written as ϕ/V_P where ϕ is the particle volume fraction. $\langle P^2(q) \rangle$ is a term including the form factor $F(q)$, a function of shape, size and particle polydispersity, and the contrast term $\Delta\rho^2$.[44] For homogeneous particles,

$$\langle P^2(q) \rangle = \langle (\rho - \rho_0)^2 V_P^2 F^2(q) \rangle \quad (2)$$

where $F(0) = 1$, and ρ and ρ_0 are the scattering length densities of the particle and of the solvent. The inner brackets represent an average weighted by the distribution of particle sizes and orientations, which is detailed as

$$\langle P^2(q) \rangle = \int_0^\infty f(R)\, dR \int_0^{\pi/2} [P(q, R, \alpha)]^2 \sin \alpha\, d\alpha \quad (3)$$

In eq 1, $S'(q)$ is the effective structure factor describing the interactions between the particles, assuming that the particle size and orientation are uncorrelated with the position of the particles.[42] $S'(q)$ is related to the structure factor $S(q)$ by the following expression:[43]

$$S'(q) = 1 + \beta(q)[S(q) - 1] \quad (4)$$

where

$$\beta(q) = \frac{\langle P(q) \rangle^2}{\langle P(q)^2 \rangle} \quad (5)$$

β is comprised between 0 and 1 and is equal to 1 for monodisperse and spherical particles. In this particular case, eq 1 becomes

$$I(q) = N_P \langle P^2(q) \rangle S(q) \quad (6)$$

In the following, β will be considered as equal to 1 as a first approximation, considering that polydispersity and orientation averaging have no effect on the structure factor factorization. The real value of β will then be discussed for model validation (see Supporting Information, part F).

For dilute systems, in the so-called Guinier region (at scales larger than the typical size of the particles), the Zimm approximation can be used to determine the scattering cross section at

zero angle $I(0)$ and the radius of gyration R_g of the particles:

$$\frac{1}{I(q)} = \frac{1}{I(0)}\left(1 + \frac{(qR_g)^2}{3}\right) \text{ for } qR_g < 1 \quad (7)$$

At $q \rightarrow 0$, eq 1 takes a simple form from which the volume of the particle V_P and the molar mass of the particle M_W can be deduced:

$$V_P = \frac{I(0)}{\phi(\rho - \rho_0)^2} \quad (8)$$

$$M_W = dN_A V_P \quad (9)$$

where d is the mass density and N_a the Avogadro number. The coherent scattering length density ρ (or SLD) expressed in eq 2 depends on the chemical composition of the particles and on the radiation source. It is calculated from the chemical composition (n) and the scattering length (b) of each atom:

$$\rho = \frac{\sum_1^N n_i b_i}{V} \quad (10)$$

where V is the volume considered in the chemical composition. While b_i regarding X-ray is proportional to the Z number of atom i, ($b_i = Z_i L_{e-}$ with $L_{e-} = 0.281 \times 10^{-12}$ cm being the scattering length of an electron), the coherent scattering length of each nucleus regarding neutron radiation is well tabulated but does not have any relation with its position on the periodic table of the elements. Moreover, the very different neutron scattering lengths of hydrogen ($b_H = -0.374 \times 10^{-12}$ cm) and deuterium ($b_D = 0.667 \times 10^{-12}$ cm) are exploited in SANS experiments for the contrast variation method.

The above description (eq 6) indicates that there are two major factors to be determined: the form factor $\langle P^2(q)\rangle$ and the structure factor $S(q)$. Various analytical form factor expressions are available to account for particle shapes. The form factor of homogeneous spheres of radius R is

$$F_S{}^2(q,R) = \left(3\frac{\sin(qR) - qR\cos(qR)}{(qR)^3}\right)^2 \quad (11)$$

For cylinders of total height H the expression of the form factor is

$$F_C{}^2(q,R) = \int_0^{\pi/2}\left[\frac{\sin((qH\cos\alpha)/2)}{(qH\cos\alpha)/2}\frac{2J_1(qR\sin\alpha)}{qR\sin\alpha}\right]^2 \sin\alpha\, d\alpha \quad (12)$$

$J_1(x)$ is the first order Bessel function, and α is the angle between the normal to the particle and the scattering vector q. Equation 12 accounts for the average on particle orientation.

For heterogeneous particles such as concentric shells or cylinders, eq 2 becomes

$$\langle P^2(q)\rangle = \langle[(\rho_S - \rho_0)V(R+\Delta R)F_\alpha(q,R+\Delta R) + (\rho_C - \rho_S)V(R)F_x(q,R)]^2\rangle \quad (13)$$

where subscripts C, S and 0 refer respectively to the core, the shell, and the solvent. R and ΔR are the radius of the core and the shell thickness, and V stands for the volume. Subscript x refers either to a sphere (eq 11) or to a cylinder (eq 12). V_P in eq 1 is equivalent here to $V(R + \Delta R)$.

The average scattering length density $\overline{\rho}$ of heterogeneous particles (e.g., core−shell) can be simply calculated at $q \rightarrow 0$ and when $S(q) = 1$, giving

$$\overline{\rho} = \frac{V(R)}{V(R+\Delta R)}\rho_C + \left[1 - \frac{V(R)}{V(R+\Delta R)}\right]\rho_S = \phi_C\rho_C + (1-\phi_C)\rho_S \quad (14)$$

where ϕ_C represents the volume fraction of the core within the particle. The particle volume and molar mass calculations seen in eqs 8 and 9 can be done replacing ρ by $\overline{\rho}$:

$$\overline{V}_P = \frac{I(0)}{\phi(\overline{\rho} - \rho_0)^2} \quad (15)$$

$$\overline{M}_W = dN_A\overline{V}_P \quad (16)$$

In the case of polydispersity, the polydisperse dimension R has to be integrated over its size distribution, $f(R)$. All size-distributed values reported here are volume average values from the log-normal distribution, according to Supporting Information, part B.

As previously mentioned, the structure factor $S(q)$ describes the interactions between the particles. In the particular case of a fractal organization, primary entities of form factor $\langle P^2(q)\rangle$ interact to form an autosimilar structure within some spatial range. A fractal object is characterized by a spatial distribution of the individual scatterers given by $N(r) \propto (r/r_0)^D$ where r_0 is the gauge of the measurement, which has the magnitude of the characteristic dimension of each individual scatterers,[45] and where D is the fractal dimension. The way particles interact in such an organization can be explored through a specific expression of the structure factor. On a wide length scale, $S(q)$ can be determined with three parameters:[45] the fractal dimension D, the cutoff distance ξ and the characteristic length scale of the individual scatterer r_0.

$$S(q) = 1 + \frac{1}{(qr_0)^D}\frac{D\Gamma(D-1)}{[1+1/(q^2\xi^2)]^{(D-1)/2}} \times \sin[(D-1)\tan^{-1}(q\xi)] \quad (17)$$

where Γ is the gamma function: $\Gamma(x) = \int_0^\infty t^{x-1}\, e^{-t}\, dt$.

Since $S(q)$ tends to unity at high q values, then $I(q)$ is dominated by the form factor of the individual scatterer (eq 6).

As described by Teixeira,[45] the meaning of ξ is only qualitative. It corresponds to the characteristic distance above which the mass distribution in the sample is no longer described by the fractal law. In other terms, it is a characteristic length scale representing the size of the cluster.[46] In comparison with Guinier's law, ξ is related to the generalized radius of gyration R_g by[45]

$$\xi^2 = \frac{2R_g{}^2}{D(D+1)} \quad (18)$$

The choice of the r_0 parameter is not direct: it is close to the radius of the individual particle, without being the exact radius. Thus, r_0 is a fitted parameter.

IV. DATA TREATMENT

For our large number of data, multiple curve fitting was performed using the SASfit software package[47] developed at the PSI (Paul Scherrer Institute, Switzerland). It is very adapted for analyzing simultaneously a large number of data which have

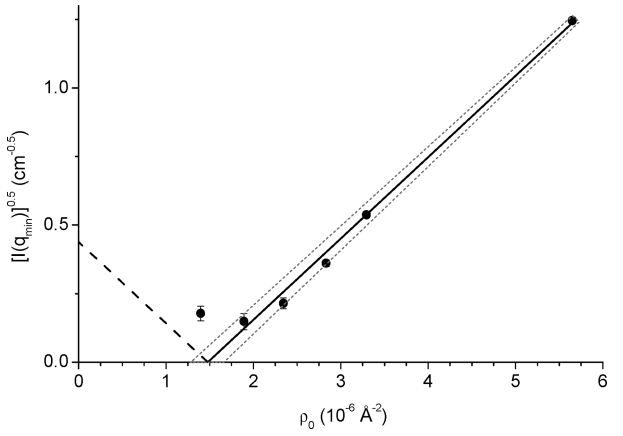

Figure 2. Plot of the square root of the scattered intensity for q_{min} (see eq 19), from the contrast variation experiment. The line shows the linear trend giving the mean SLD at *x*-axis intersection.

same geometry and composition parameters, however different scaling conditions. Variables can be set as local (specific for each spectrum fitted) or global (common for every spectra), in order to make a restrictive system. This methodology for data analysis is powerful for describing complex systems.

Multiple curve fitting enabled determination of the geometric parameters and composition of the particles. Input experimental data were neutron spectra at various solvent conditions and an X-ray spectrum, seven conditions in total. $I(q)/S(q)$ spectra were fitted to $N_P\langle P^2(q)\rangle$ (eq 6), $\langle P^2(q)\rangle$ being a core−shell sphere and a core shell cylinder form factor (eq 13) and $S(q)$ a mass-fractal structure factor (eq 17). The parameters are described in the Table SC2 in the Supporting Information. Geometric parameters (R, σ, ΔR, H) were global parameters for the seven solvent conditions, contrary to the core and shell SLDs, which were local, in order to detect any solvent penetration in the core or in the shell.

As described in Supporting Information, part C, $S(q)$ was calculated for various values of r_0. The fitting routine was performed for each r_0 value, and an optimal r_0 was found.

V. RESULTS AND DISCUSSION

The successful study of such a complex system was done by multiplying the data sets from several techniques and in various conditions, reaching absolute scaling, analyzing a large length scale, and introducing restrictive conditions by multiple fitting, in order to limit the number of potential solutions and to increase the selectivity of the resulting model.

1. Scattering Length Density Calculation. Working with an absolute intensity scale enables consideration of the composition of the particles, via their scattering length density (SLD). Asphaltene SLD regarding neutron and X-ray can be calculated from the chemical composition (Table 1) with eq 10. SLD values are 1.41×10^{-6} Å^{-2} for neutron scattering, and 1.09×10^{-5} Å^{-2} for X-ray scattering. Besides, neutron contrast variation is an experimental technique to measure the average SLD. Equation 6 at $q \rightarrow 0$ becomes

$$I(q \rightarrow 0) = (\overline{\rho} - \rho_0)^2 \overline{N}_P \overline{V}_P{}^2 S(q \rightarrow 0) \qquad (19)$$

When varying ρ_0 in a contrast variation experiment, $\overline{\rho}$, the average asphaltene SLD, is determined when the minimum of intensity is reached. Figure 2 shows the square-root of the measured intensity $I(q_{min})$ (see eq 19) as a function of the solvent SLD (ρ_0). The samples were 50 g/L asphaltene solutions in toluene at various H/D ratios. According to our experiments, q_{min} was chosen as the smallest q value where scattered intensity was measured (q_{min} = 0.06 Å^{-1}). It should be profitable to measure the intensity at smaller q values to better respect the approximation $q \rightarrow 0$. Nevertheless, Figure 2 shows a nice expected behavior of the scattered intensity which can be further interpreted.

The linear decrease of the square root of the intensity as ρ_0 decreases allows a reasonably good extrapolation giving rise to the average SLD value. The minimum scattered intensity is reached at $\overline{\rho} = (1.5 \pm 0.2) \times 10^{-6}$ Å^{-2}. This experimental result is in very good agreement with the average SLD calculated from the asphaltene chemical composition (1.41×10^{-6} Å^{-2}). In consequence, it validates the calculation carried out from chemical composition, which is particularly interesting regarding X-ray scattering, for which there is no experimental way to measure the SLD.

2. Modeling SAXS, SANS and Contrast Variation Spectra. As mentioned in the Introduction, asphaltenes have been described as mass fractal aggregates.[27,28] Modeling their small angle scattering spectrum on an extended length scale requires finding the parameters of the form factor describing the individual particles, and the structure factor, corresponding to the interaction between the individual particles (eq 6).

Structure Factor Determination. The fractal state can be described in terms of interactions between the individual particles, known as the structure factor $S(q)$. The $S(q)$ expression adapted for fractal structure is detailed in eq 17. With the intention of studying the fine structure of asphaltenes at small length scale, i.e. the form factor of the small objects in eq 6, the structure factor for asphaltene fractals can be estimated, choosing adequate D, ξ and r_0 (eq 17).

The fractal dimension D is set at 2.1, regarding the work done by Barré et al.[27] The cutoff distance ξ, which is linked to the size of the aggregate, is carried out from eq 18: the radius of gyration is measured from the Zimm approximation applied on the neutron and X-ray spectra of Figure 1 (71 ± 1 Å). The calculation gives ξ = 40 Å. r_0, which is the characteristic dimension of the individual particle, is part of the fitting procedure (see Supporting Information, part C), which gives r_0 = 18 Å. The effect of r_0 on the resulting parameters extracted from the following multiple fits are shown in Supporting Information, part C.

The experimental scattering spectra of the asphaltene solution can be divided by the estimated fractal $S(q)$. The resulting curves answer to $I(q)/S(q) = N_P\langle P^2(q)\rangle$. One has now access to the experimental form factor of the individual particles.

Form Factor Determination. Multiple curve fitting was implemented for describing with precision the dimensions and the composition of the nanoaggregate, via the form factor. The results of these multiple fits are shown in Figure 3. The seven spectra were separated into two graphs for clarity. The X-ray spectrum was well fitted by both sphere and cylinder core−shell geometries: the fitted curves cannot be distinguished from the experimental data points in Figure 3. But regarding neutrons, it clearly demonstrates that the core−shell cylinder geometry gives relatively good fits for all solvent conditions, contrary to the core−shell sphere geometry. The dimensions (Table 2) of the cylinder geometry reveal that the particles are best described by core−shell flat disks.

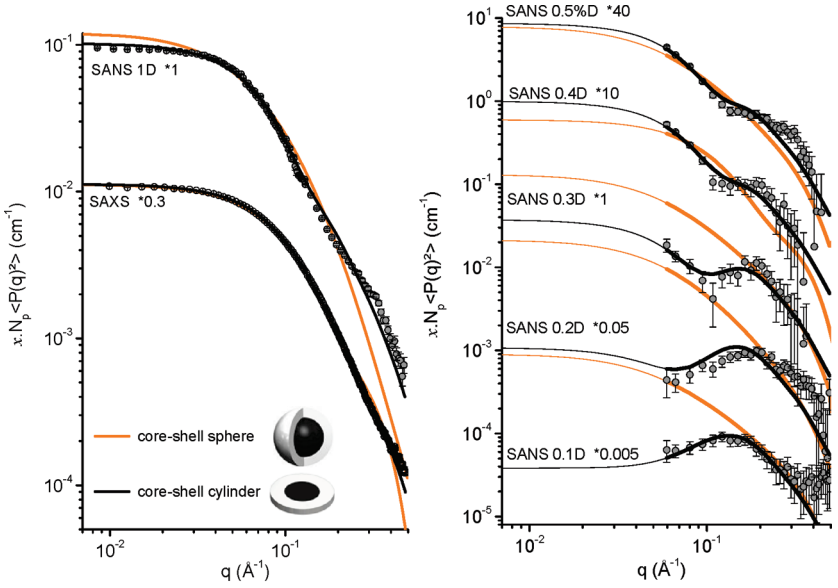

Figure 3. (symbols) (a) SAXS and SANS 100% D (5 g/L in H- and D-toluene respectively) and (b) SANS contrast variation (50 g/L in toluene at various H/D ratios) asphaltene spectra divided by $S(q)$. (lines) Fits with (i) core−shell sphere form factor; (ii) core−shell cylinder form factor. Spectra are rescaled for sake of clarity.

Table 2. Parameters Extracted from the Fits Shown in Figure 3

	symbol	unit	core−shell sphere	core−shell cylinder
	χ^2		1125	188
radius of the core	R	Å	20.2	18.2
polydispersity of the core	σ		0.55	0.30
thickness of the shell	ΔR	Å	9.6	14.4
height	H	Å		6.7

The SLDs of the core and of the shell for the two geometries are plotted in Figure 4a versus the solvent SLD. The average SLD is calculated with eq 14 and shown for each solvent condition. The asphaltene SLD, calculated according to eq 10 from the asphaltene chemical composition, is represented by the lines on the graph. On the whole, we observe in Figure 4a that the core and the shell are contrasted. The values at $\rho_0 = 5.65 \times 10^{-6}$ Å^{-2}, corresponding to the 100% D solvent, have a low precision because of the low contrast with the solvent. The contrast variation technique is well justified. Concerning the results from the core−shell cylinder form factor and regarding neutrons, ρ_C is comprised between 3 and 5×10^{-6} Å^{-2} while ρ_S is between 0.2 and 1.5×10^{-6} Å^{-2}. The average SLD, $\overline{\rho}$, between 1.5 and 1.9×10^{-6} Å^{-2}, is close to the line at 1.41×10^{-6} Å^{-2}, corresponding to the SLD known from the chemical composition. Regarding X-rays, ρ_C is 13.7×10^{-6} Å^{-2} while ρ_S is 8.5×10^{-6} Å^{-2}. The average SLD, $\overline{\rho}$, is calculated at 1.01×10^{-6} Å^{-2}, close to the line at 1.09×10^{-6} Å^{-2}.

These observations made on SLDs enable discussion of how close the model is to reality. The cylinder geometry expresses an average SLD close to the asphaltene average composition, both for neutrons and for X-rays. The core−shell sphere geometry, on the contrary, gives SLD values much more removed from average SLDs, especially regarding X-ray (see Figure 4a).

Apart from the χ^2 values (Table 2), expressing the quality of the fit, the results on average SLDs bring subsequent support to the core−shell cylinder model, and lead us to reject the sphere model.

SLD profiles in Figure 4b clearly show that, for X-rays, the shell presents a very low contrast with the solvent. Consequently, X-rays mostly see the core, but are not sensitive to the shell. On the contrary, the deuterated solvent offers a high contrast for both core and shell, regarding neutrons.

The contrast variation experiment enables discussion about the solvatation of the particles. When increasing the H/D ratio (i.e., decreasing ρ_0), Figure 4 illustrates that the scattering length density of the shell of the nanoaggregate does not decrease drastically, as it would be observed for a solvated shell. This relevant finding shows that there is no or low solvent penetration in the shell. The same observation is made for the core.

3. Discussions. The results combining X-ray, neutron scattering and contrast variation experiment showed that asphaltenes are best described by core−shell cylinder-like particles, organized as mass fractal aggregates. The form of the asphaltene nanoaggregate, its dimensions and chemical composition deduced from the small angle scattering experiments, can be compared with the current description of the asphaltene molecular structure.

Mass of the Nanoaggregate. The extrapolation of the scattered intensity at q tending to zero, $I(q \to 0)$, calculated from curve fitting, enables calculation of the volume and the average molar mass of one particle (eq 16). The volume of the described nanoaggregate is 22×10^3 Å^3, and its molecular weight is 16×10^3 Da.

If we consider that the molecular weight of the asphaltene molecule is around 750 ± 250 g/mol,[3] the here described nanoaggregate accounts for about 20 ± 5 elementary molecules. In comparison, aggregation numbers reported in the literature by ^{1}H NMR, gravitational gradients and conductimetry measurements[19,21,25] are around 8.

Global Geometry and Dimensions. This disk geometry is analogous to aromatic sheet stacking, only observed

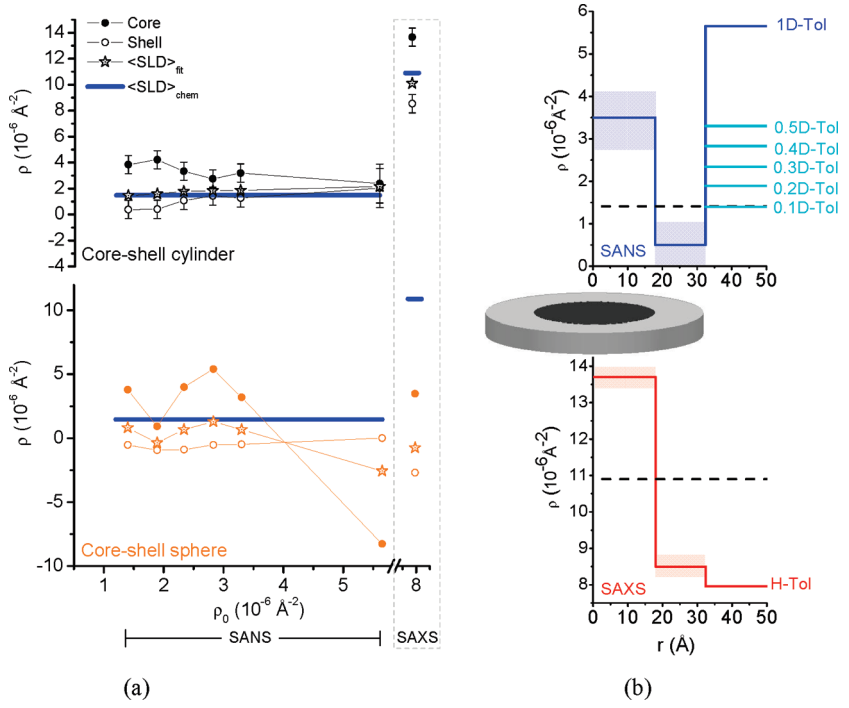

Figure 4. (a) Scattering length densities given by the multiple fits of Figure 3, of the core and of the shell vs solvent SLD. $\langle SLD \rangle_{fit}$ is the average SLD, sum of the core and the shell SLD weighted by their volume (eq 14). $\langle SLD \rangle_{chem}$ is the asphaltene SLD calculated from chemical composition (eq 10). (b) SLD profiles for the core−shell cylinder geometry, regarding neutrons and X-rays, from the results shown in panel a. The dashed line expresses $\langle SLD \rangle_{chem}$.

experimentally on dry asphaltenes,[7] and assessed by molecular simulation work on asphaltene aggregation.[10−12] According to the Yen model,[7] X-ray diffraction data (XRD) on dry asphaltenes have shown a stacking thickness between 14 and 28 Å. The distance between neighboring aromatic sheets was found to be in the range 3.55 to 3.70 Å from XRD data. The calculated number of stacking sheets is between 4 and 8. Here, we report a 6.7 Å disk height, which is rather low compared to dry asphaltene data. Nevertheless, our scattering experiments deal with asphaltene solutions, and a more extended stacking of nanoaggregates can be auspicious for solid asphaltenes. There, the height accounts for 2 to 3 aromatic stacks, if we consider the distance between two sheets analogous to a graphite organization. The modified Yen model[26] considers an aggregation number of 6 nanoaggregates from DC conductivity and diffusion coefficient measurements, without directly making allowance for aromatic stacking. We show in Supporting Information, part G, the dimensions obtained from the multiple fits when we set a stacking number of 6, corresponding to H = 17 Å. From spectra fitting, the core becomes twice smaller and the shell thickness doubles. This solution does not seem realistic for aromatic stacking to occur. Recent relevant molecular dynamics simulations in solvent solutions were conducted by Headen et al.[48] who have observed the formation of dimers and trimers of asphaltene molecules in toluene. These findings are in good agreement with our experimental results.

Apart from the height, we describe a total radius of 32 Å for the nanoaggregate. The average core radius, 18 Å, is bigger than the extended sheet proposed by the Yen model, reported between 8 and 15 Å. This core is also larger than the size of the PAH of the molecule proposed by the modified Yen model,[26] making reference to a 7-fused ring system, thus to a core radius of ∼5 Å. The polydispersity parameter discussed here is additional information compared to previous studies on asphaltene nanoaggregates. Introduced by a log-normal law on the core radius, σ is 0.30. This value is rather low for a natural material.

From such dimensions and geometry we can calculate the particle diffusion coefficient, useful to compare to the results reported from hydrodynamics. We have used the modified Stokes−Einstein equation (see Supporting Information, part D) adapted for a cylindrical particle in a solvent. Two main terms must be assessed in this equation: (i) the friction coefficient (f_s) was calculated according to the equation for the oblate ellipsoid model,[49] (ii) and the hydrodynamic radius was estimated from the expression proposed by Mazer et al.[50] for a cylindrical particle (a, the semimajor axis, and b, the semiminor axis; see Supporting Information, part D). Using volume average dimensions, the calculation gives a diffusion coefficient of $(1.0 \pm 0.2) \times 10^{-10}$ m^2/s for asphaltene nanoaggregates in toluene at low concentration. This value falls within the bottom range of diffusion coefficients given by other techniques such as NMR, centrifugation, impedance, and QCM-D,[13,15−17,20−24] between 1 and 4 × 10^{-10} m^2/s in the same conditions.

Core−Shell Composition. The results obtained from the multiple fits enables descrition of the core and the shell of the nanoaggregate, via their volume and SLD (Table 2 and Figure 4). The average SLD was calculated with eq 10 from these parameters and showed that it was close to the asphaltene SLD known from chemical composition (Figure 4). In addition, eq 10 can be reversed to determine the chemical composition of the particle when SLD and volume are known parameters. Average composition— via the H/C ratio—thus obtained can be compared to the experimental values of Table 1, constituting a final argument for model validation. This was done combining X-ray

dx.doi.org/10.1021/jp111468d |J. Phys. Chem. B 2011, 115, 6827–6837

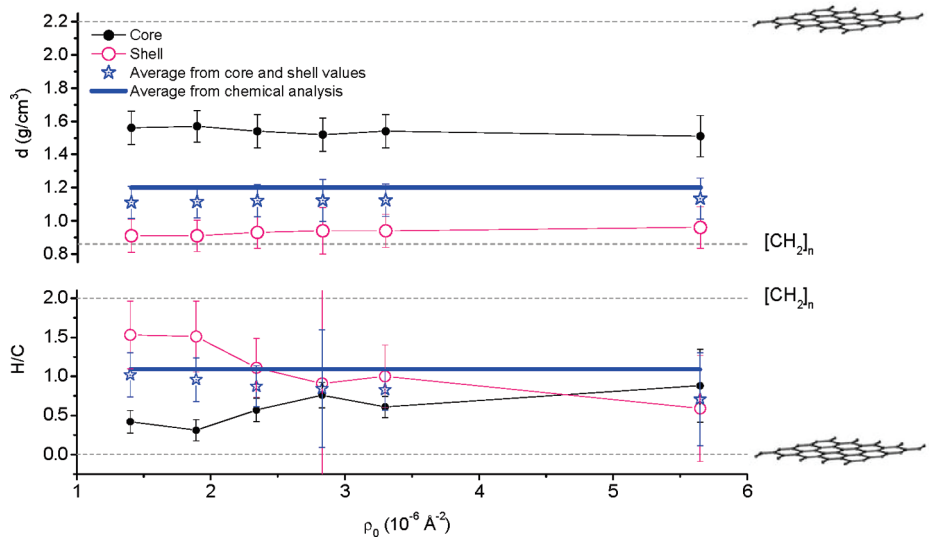

Figure 5. Core and shell chemical description carried out from the geometrical and compositional core−shell cylinder model spawned by SANS and SAXS data treatment. Results (mass density; H/C ratio) are shown for each solvent condition. The horizontal lines correspond to the values given by chemical characterization (Table 1). Extreme values (dash) are illustrated by their corresponding atomic organization (graphene and alkane).

and neutron scattering data. Asphaltenes were considered as only made of carbon and hydrogen, because due to the low proportion (Table 1), heteroatoms do not contribute much to the contrast. H/C values and mass densities (d) of the core, the shell, and average values were calculated, following the sets of equations in the Supporting Information, part E.

Figure 5 shows the results for each solvent condition for the core, the shell and the average particle. Although H/C values are provided with large error bars, the graph globally highlights an aromatic core, with an H/C ratio around 0.5, and a density of 1.6 g/cm^3. On the contrary, the shell offers a higher H/C ratio, between 1 and 1.6, showing a less aromatic region, more concentrated in alkyl chains. The mass density of the shell is rather high for aliphatics, around 0.93 g/cm^3, which shows that the shell is not made of normal alkanes but rather unsaturated alkanes. The average H/C ratio is reasonably close to the ratio given by chemical composition, and the calculated average mass density is in good agreement with the measured density (see Figure 5 and Table 1). These remarks are strong arguments toward the model validation.

The composition contrast between the core and the shell is shown, although the core is not representative of a pure aromatic structure. We find a low density compared to graphene (1.6 against 2.2 g/cm^3), and the H/C ratio is relatively high for aromatic structure (0.5). The presence of naphthenic rings or metalloporphyrins inside the core would indeed increase the H/C ratio and decrease the density, while conserving the rigidity of the structure.

Molecular Structure. SAXS and SANS measurements do not give any information on molecular structure, though one must be careful not to overinterpret these results. However, from composition, density and sizes, and from literature reviews on asphaltene molecular structure,[26] we can attempt some presumptions. The composition-contrasted nanoaggregate, made of an aromatic core and an aliphatic shell, is analogous to the island model of asphaltene molecules. But, regarding its density and H/C ratio, the core must contain naphthenic rings and/or heteroatoms, which does not diverge from the described island model. Additionally, the disk shape is equivalent to aromatic stacking, made of $\pi-\pi$ association of island molecules. But the core is much bigger than the asphaltene PAH proposed, 18 Å against 5 Å. According to that, one single molecule cannot account for one stack. Moreover, the mass of the nanoaggregate, related to the molecular weight,[26] gives an aggregation number of 20 ± 5, which again is a lot higher than the reported aggregation number of 6 molecules per nanoaggregate.[26] These discrepancies deserve consideration for enriching the nanoaggregate description.

Presence of Heteroatoms. Apart from carbon and hydrogen in high proportion, asphaltenes contain some heteroatoms, mainly sulfur (Table 1). The effect of sulfur on the H/C ratio and on mass density was assessed. Assuming that sulfur is mostly present in the surrounding parts of the molecule,[39] all sulfur atoms were considered in the shell. Modifications on eq E2 (see Supporting Information, part E) introducing sulfur compound did not have a major effect on the H/C ratio of the shell, neither on the mass density, within experimental uncertainty.

Another important result is given by the contrast variation experiment. Figure 4 reveals no variation of the core and shell scattering length densities as the H/D ratio of the solvent mixture is changed: solvent penetration is unlikely. The fact that the shell does not contain any solvent means that it is a rather dense shell, where alkyl chains prevent the solvent to get into the nanoaggregate. Indeed this is what the mass density tells us: the density of the shell is high compared to the density of normal alkanes (0.75 g/cm^3 for dodecane).

Stacking Limit. The main driving force of this nanoaggregate building is the strong interaction between aromatic sheets. The limit in aggregation number is often observed by molecular simulation[51] because of steric repulsion brought from the aliphatic branches making the shell. The composition of the shell could enable confirmation of this steric hindrance. Considering the number of carbons in the shell, n_{Cs}, calculated from eq E2 in the Supporting Information, and the volume of the shell from the geometric parameters, we can determine V_C, the volume occupied by one carbon atom in the shell: $V_C = (1/n_{Cs})\pi H[(R + \Delta R)^2 - R^2]$. We find $V_C = 23.6$ Å^3. This value can be compared to

Figure 6. Illustration of the core−shell nanoaggregate, with the shell made of aliphatic chains presenting a roll around the core.

the volume occupied by a CH_2 in the liquid phase: 30 Å^3.[52] In order to reach this volume occupation, the shell should be 1.7 Å higher than the value of H obtained from SAXS and SANS spectra fitting, meaning that the shell would present a small roll around the core, according to Figure 6. As observed, this roll is not very consequent and would probably not avoid a new aromatic sheet to approach. But if we consider the shell being made not only of aliphatic hydrocarbon but rather of branched chains or even of some naphthenic rings, V_C will be higher and the branches would be even less flexible. A new stack would less probably reach the optimal distance for strong $\pi-\pi$ interaction. These analytical results on core and shell composition could be the starting point for further understanding on the limit of the aromatic stacking.

We have highlighted the formation of much larger aggregates having a fractal structure, but of finite diameter. Nevertheless, the origin of these interactions involved in this large macrostructure building is not well understood, nor is the limit in fractal aggregation. A thorough understanding of this macroaggregation needs to explore the variation and the form of the $S(q)$ term, reducing polydispersity, or inducing asphaltene solution perturbations, obtained by increasing temperature or changing the solvent.

Model Limits. The first and unambiguous limit to the model concerns the experimental data. The relevant length scale for this study is acquired at high q values, where low scattering intensity from the sample is recorded. Even with a careful experimentation (sample preparation, solvent purification, adapted concentrations, long time exposures, and so on), particle scattering has to be carefully extracted from background noise and incoherent scattering. Incoherent background, inherent to high asphaltene concentration, introduces some limits to the interpretation of the high q data, even when subtracted from the signal (see Supporting Information, part A).

The estimation of the structure factor comes into the picture of the nanoaggregate description, because the fitted data depend on this fractal structure factor. As previously described, $S(q)$ is determined from three parameters. The characteristic size of the individual scatterer, r_0, is equivocal. As detailed in the Supporting Information, part C, r_0 was taken as the one giving the best fits for the multiple data treatment, although the value chosen does impact the final result within some range. The effect of r_0 on each parameter can be found in the Supporting Information, part C. As observed, the major conclusions on the geometry, dimensions and particle organization are only weakly affected when changing r_0 in the considered domain of analysis.

The contrast variation experiment was conducted at high concentration, because the high q-data range, associated with low intensities, was analyzed. At this concentration, previous experiments have shown that interactions between clusters are nonnegligible. Rigorously, a structure factor describing how clusters are organized should be considered, particularly in the low q range. For contrast variation, only the very high q range was spawned, where this additional structure factor should be close to 1.

The results have shown that the nanoaggregate is an anisotropic and polydisperse particle. It means that, regarding eq 1, an effective structure factor $S'(q)$ has to be considered, introducing the β ratio (eq 4). To observe the effect of anisotropy and polydispersity on $S'(q)$, β was calculated regarding the core−shell cylinder form factor described from the multiple fit (Figure 3), for neutron and X-ray scattering. The steps and results of the calculation are shown in Supporting Information, part F: Figure SF1 compares $I(q)/S(q)$ and $I(q)/S'(q)$ for SANS and SAXS, showing the decoupling approximation effect. Anisotropy and polydispersity effects would have to be accounted for in the determination of β but do not change the conclusions proposed in this study.

Through this approach, SLD profiles are shown to be sharp and angular (see Figure 4b). Experimental data should be better reproduced using smoother profiles, like tooth and bell profiles for neutron and X-ray respectively. Such profiles are however more difficult to implement in a fitting procedure. We believe that introducing a polydispersity on the core is equivalent to implementing smooth profiles. Another approach, working on the pair function distribution, would be complementary to this work.[53]

Model Selectivity. Despite subsequent limits that have to be taken into account, this model offers a great selectivity from several points of view. First, the comparison of neutron and X-ray scattering data gives unequivocal results. These two techniques have a strong potential because they observe the same length scale but from two different views. Similarly to contrast variation techniques, the simultaneous analysis of the SAXS and SANS patterns at various solvent conditions increases the number of extractable parameters, thus enabling limitation of the number of potential solutions. The second strength of this study comes from the great set of scattering data that was accounted for, and the large q range analyzed. These conditions highly increase the selectivity of the resulting model. Moreover, the multiple fitting procedure employed enables finding one set of parameters best accounting for all spectra. It is a highly restrictive system, which is required for such a complex mixture. Eventually, considering the composition parameters is one of the best advances in this model fitting: the objective functions fitted were defined without any scaling factor.

VI. CONCLUSION

Asphaltene nanoaggregates are largely discussed in the literature, but their description in terms of shape and composition often lacks of experimental data. As asphaltenes are described by aggregation mechanisms on a large length scale, a technique that allows observation on a wide length scale is needed. In this work, we have shown that coupled techniques such as neutron and X-ray small angle scattering and precise measurements via absolute scaling enable unraveling of the asphaltene nanoaggregate structure and acquisition of rich and detailed information. This study highlights a fractal structure at large length scale, made by the aggregation of small entities represented by core−shell disks at small length scale. Data treatment combining shape fitting and absolute scaling through chemical composition showed that the sphere model did not account for the nanoaggregate shape, contrary to the disk shape. A contrast variation technique gave insight into core and shell compositions. We have to underline the very coherence between the results given by these different approaches, which finally thoroughly validates the nanoaggregate model. Both dimension and composition results are globally in good agreement with the Yen and modified Yen models and with literature data, representing the nanoaggregate by a dense aromatic core and a shell highly concentrated in aliphatic carbon.

From the detailed description of the nanoaggregate, accounting for a molecular organization by aromatic stacking and limited

by steric repulsion from the peripheral chains, further aggregation mechanisms into the fractal structure can be investigated. The structure factor introduced in this work is the key for a better understanding of this complex organization.

■ ASSOCIATED CONTENT

Supporting Information. Incoherent subtraction; size average calculations; multiple curve fitting for the determination of r_0; calculation of the diffusion coefficient; chemical composition determination from scattering parameters; decoupling approximation for polydisperse anisotropic particles; and variation on disk height. This material is available free of charge via the Internet at http://pubs.acs.org.

■ AUTHOR INFORMATION

Corresponding Author
*E-mail: loic.barre@ifpen.fr.

■ ACKNOWLEDGMENT

The authors want to thank J. Kohlbrecher and I. Bressler from the Paul Scherrer Institute (Switzerland) for their very useful SASfit software, containing a large number of functions which offer great possibilities. We are grateful for the time they spent on adapting a new version of their software for the purpose of this analysis.

■ REFERENCES

(1) Sheu, E. Y. Petroleum asphaltene-properties, characterization, and issues. *Energy Fuels* **2002**, *16*, 74–82.
(2) Verdier S. Experimental Study and Modelling of Asphaltene Precipitation Caused by Gas Injection. PhD, Technical University of Denmark, 2006.
(3) *Asphaltenes, Heavy Oils and Petroleomics*; Mullins, O. C., Sheu, E. Y., Hammami, A., Marshall, A. G., Eds.; Springer: New York, 2007.
(4) Groenzin, H.; Mullins, O. C. Asphaltene molecular size and weight by time-resolved fluorescence depolarization. In *Asphaltenes, Heavy Oils and Petroleomics*; Mullins, O. C., Sheu, E. Y., Hammami, A., Marshall, A. G., Eds.; Springer: New York, 2007; Chapter 2, p 17.
(5) Strausz, O. P.; Mojelsky, T. W.; Lown, E. M. The Molecular-Structure of Asphaltene—An Unfolding Story. *Fuel* **1992**, *71*, 1355–1363.
(6) Yen, T. F. The colloidal aspect of a macrostructure of petroleum asphalt. *Fuel Sci. Technol. Int.* **1992**, *10*, 723–733.
(7) Yen, T. F.; Erdman, J. G.; Pollack, S. S. Investigation of the Structure of Petroleum Asphaltenes by X-Ray Diffraction. *Anal. Chem.* **1961**, *33*, 1587–1594.
(8) Tanaka, R.; Sato, E.; Hunt, J. E.; Winans, R. E.; Sato, S.; Takanohashi, T. Characterization of asphaltene aggregates using X-ray diffraction and small-angle X-ray scattering. *Energy Fuels* **2004**, *18*, 1118–1125.
(9) Wiehe, I. A.; Liang, K. S. Asphaltenes, resins, and other petroleum macromolecules. *Fluid Phase Equilib.* **196**, No. 117, 201–210.
(10) Murgich, J.; Rodriguez, J.; Aray, Y. Molecular recognition and molecular mechanics of micelles of some model asphaltenes and resins. *Energy Fuels* **1996**, *10*, 68–76.
(11) Rogel, E. Studies on Asphaltene Aggregation Via Computational Chemistry. *Colloids Surf., A* **1995**, *104*, 85–93.
(12) Rogel, E. Thermodynamic modeling of asphaltene aggregation. *Langmuir* **2004**, *20*, 1003–1012.
(13) Andreatta, G.; Bostrom, N.; Mullins, O. C. High-Q ultrasonic determination of the critical nanoaggregate concentration of asphaltenes and the critical micelle concentration of standard surfactants. *Langmuir* **2005**, *21*, 2728–2736.
(14) Goncalves, S.; Castillo, J.; Fernandez, A.; Hung, J. Absorbance and fluorescence spectroscopy on the aggregation behavior of asphaltene-toluene solutions. *Fuel* **2004**, *83*, 1823–1828.
(15) Goual, L. Impedance Spectroscopy of Petroleum Fluids at Low Frequency. *Energy Fuels* **2009**, *23*, 2090–2094.
(16) Lisitza, N. V.; Freed, D. E.; Sen, P. N.; Song, Y. Q. Study of Asphaltene Nanoaggregation by Nuclear Magnetic Resonance (NMR). *Energy Fuels* **2009**, *23*, 1189–1193.
(17) Mostowfi, F.; Indo, K.; Mullins, O. C.; McFarlane, R. Asphaltene Nanoaggregates Studied by Centrifugation. *Energy Fuels* **2009**, *23*, 1194 1200.
(18) Sheu, E. Y. *Petroleomics and characterization of asphaltene aggregates using small angle scattering*; Mullins, O. C., Sheu, E. Y., Hammami, A., Marshall, A. G., Eds.; Springer: New York, 2007; Chapter 14, p 353.
(19) Zeng, H.; Song, Y. Q.; Johnson, D. L.; Mullins, O. C. Critical Nanoaggregate Concentration of Asphaltenes by Direct-Current (DC) Electrical Conductivity. *Energy Fuels* **2009**, *23*, 1201–1208.
(20) Abudu, A.; Goual, L. Adsorption of Crude Oil on Surfaces Using Quartz Crystal Microbalance with Dissipation (QCM-D) under Flow Conditions. *Energy Fuels* **2009**, *23*, 1237–1248.
(21) Betancourt, S. S.; Ventura, G. T.; Pomerantz, A. E.; Viloria, O.; Dubost, F. X.; Zuo, J. L.; Monson, G.; Bustamante, D.; Purcell, J. M.; Nelson, R. K.; Rodgers, R. P.; Reddy, C. M.; Marshall, A. G.; Mullins, O. C. Nanoaggregates of Asphaltenes in a Reservoir Crude Oil and Reservoir Connectivity. *Energy Fuels* **2009**, *23*, 1178–1188.
(22) Durand, E.; Clemancey, M.; Lancelin, J. M.; Verstraete, J.; Espinat, D.; Quoineaud, A. A. Aggregation States of Asphaltenes: Evidence of Two Chemical Behaviors by H-1 Diffusion-Ordered Spectroscopy Nuclear Magnetic Resonance. *J. Phys. Chem. C* **2009**, *113*, 16266–16276.
(23) Indo, K.; Ratulowski, J.; Dindoruk, B.; Gao, J. L.; Zuo, J. L.; Mullins, O. C. Asphaltene Nanoaggregates Measured in a Live Crude Oil by Centrifugation. *Energy Fuels* **2009**, *23*, 4460–4469.
(24) Kawashima, H.; Takanohashi, T.; Iino, M.; Matsukawa, S. Determining Asphaltene Aggregation in Solution from Diffusion Coefficients As Determined by Pulsed-Field Gradient Spin-Echo H-1 NMR. *Energy Fuels* **2008**, *22*, 3989–3993.
(25) Freed, D. E.; Lisitza, N. V.; Sen, P. N.; Song, Y. Q. *Asphaltene molecular composition and dynamics from NMR diffusion measurements*; Mullins, O. C., Sheu, E. Y., Hammami, A., Marshall, A. G., Eds.; Springer: New York, 2007; Chapter 11, p 353.
(26) Mullins, O. C. The Modified Yen Model. *Energy Fuels* **2010**, *24*, 2179–2207.
(27) Barre, L.; Simon, S.; Palermo, T. Solution properties of asphaltenes. *Langmuir* **2008**, *24*, 3709–3717.
(28) Fenistein, D.; Barre, L.; Broseta, D.; Espinat, D.; Livet, A.; Roux, J. N.; Scarsella, M. Viscosimetric and neutron scattering study of asphaltene aggregates in mixed toluene/heptane solvents. *Langmuir* **1998**, *14*, 1013–1020.
(29) Fenistein, D.; Barre, L. Experimental measurement of the mass distribution of petroleum asphaltene aggregates using ultracentrifugation and small-angle X-ray scattering. *Fuel* **2001**, *80*, 283–287.
(30) Gawrys, K. L.; Kilpatrick, P. K. Asphaltenic aggregates are polydisperse oblate cylinders. *J. Colloid Interface Sci.* **2005**, *288*, 325–334.
(31) Roux, J. N.; Broseta, D.; Deme, B. SANS study of asphaltene aggregation: Concentration and solvent quality effects. *Langmuir* **2001**, *17*, 5085–5092.
(32) Thiyagarajan, P.; Hunt, J. E.; Winans, R. E.; Anderson, K. B.; Miller, J. T. Temperature-Dependent Structural-Changes of Asphaltenes in 1-Methylnaphthalene. *Energy Fuels* **1995**, *9*, 829–833.
(33) Herzog, P.; Tchoubar, D.; Espinat, D. Macrostructure of Asphaltene Dispersions by Small-Angle X-Ray-Scattering. *Fuel* **1988**, *67*, 245–250.
(34) Sheu, E. Y.; Liang, K. S.; Sinha, S. K.; Overfield, R. E. Polydispersity Analysis of Asphaltene Solutions in Toluene. *J. Colloid Interface Sci.* **1992**, *153*, 399–410.
(35) Tanaka, R.; Hunt, J. E.; Winans, R. E.; Thiyagarajan, P.; Sato, S.; Takanohashi, T. Aggregates structure analysis of petroleum asphaltenes with small-angle neutron scattering. *Energy Fuels* **2003**, *17*, 127–134.

(36) Gawrys, K. L.; Blankenship, G. A.; Kilpatrick, P. K. Solvent entrainment in and flocculation of asphaltenic aggregates probed by small-angle neutron scattering. *Langmuir* **2006**, *22*, 4487–4497.
(37) Sheu, E. Y. Small angle scattering and asphaltenes. *J. Phys.: Condens. Matter* **2006**, *18*, S2485–S2498.
(38) Barre, L.; Espinat, D.; Rosenberg, E.; Scarsella, M. Colloidal structure of heavy crudes and asphaltene solutions. *Rev. Inst. Fr. Pet.* **1997**, *52*, 161–175.
(39) Barre, L.; Jestin, J.; Morisset, A.; Palermo, T.; Simon, S. Relation between Nanoscale Structure of Asphaltene Aggregates and their Macroscopic Solution Properties. *Oil Gas Sci. Technol.* **2009**, *64*, 617–628.
(40) Khvostichenko, D. S.; Andersen, S. I. Interactions between asphaltenes and water in solutions in toluene. *Energy Fuels* **2008**, *22*, 3096–3103.
(41) Grillo I. SANS and Applications in Soft Condensed Matter. In *Soft Matter Characterization*; **2008**; Chapter 13, p 723.
(42) Hayter, J. B.; Penfold, J. Determination of Micelle Structure and Charge by Neutron Small-Angle Scattering. *Colloid Polym. Sci.* **1983**, *261*, 1022–1030.
(43) Kotlarchyk, M.; Chen, S. H. Analysis of Small-Angle Neutron-Scattering Spectra from Polydisperse Interacting Colloids. *J. Chem. Phys.* **1983**, *79*, 2461–2469.
(44) Please note that for convenience, the function P is different from the usual notation where $P(q) = F^2(q)$.
(45) Teixeira, J. Small-Angle Scattering by Fractal Systems. *J. Appl. Crystallogr.* **1988**, *21*, 781–785.
(46) Sorensen, C. M. Light scattering by fractal aggregates: A review. *Aerosol Sci. Technol.* **2001**, *35*, 648–687.
(47) Kohlbrecher, J.; Bressler, I. SASfit customized version of version 0.93.2 available at http://kur.web.psi.ch/sans1/SANSSoft/sasfit.html.
(48) Headen, T. F.; Boek, E. S.; Skipper, N. T. Evidence for Asphaltene Nanoaggregation in Toluene and Heptane from Molecular Dynamics Simulations. *Energy Fuels* **2009**, *23*, 1220–1229.
(49) Perrin, F. Mouvement brownien d'un ellipsoïde (II). *J. Phys. Radium* **1936**, *1*, 11.
(50) Mazer, N. A.; Benedek, G. B.; Carey, M. C. Quasi-Elastic Light-Scattering-Studies of Aqueous Biliary Lipid Systems—Mixed Micelle Formation in Bile-Salt Lecithin Solutions. *Biochemistry* **1980**, *19*, 601–615.
(51) Murgich, J. Molecular simulation and the aggregation of the heavy fractions in crude oils. *Mol. Simul.* **2003**, *29*, 451–461.
(52) Small, D. M. The Physical Chemistry of Lipids: From Alkanes to Phospholipids. In *Handbook of Lipid Research*; Small, D. M., Ed.; Springer: New York, 1986; Chapter 7.
(53) Brunner-Popela, J.; Glatter, O. Small-angle scattering of interacting particles. 1. Basic principles of a global evaluation technique. *J. App. Crystallogr.* **1997**, *30*, 431–442.